Article:
Mangan, TP orcid.org/0000-0001-7053-5594, Harman-Thomas, JM, Lade, RE et al. (2 more authors) (2020) Kinetic study of the reactions of AlO and OAlO relevant to planetary mesospheres. ACS Earth and Space Chemistry, 4 (11). pp. 2007-2017. ISSN 2472-3452

https://doi.org/10.1021/acsearthspacechem.0c00197

Kinetic study of the reactions of AlO and OAlO relevant to planetary mesospheres

Thomas P. Mangan[1], James M. Harman-Thomas[1+], Rachel E. Lade[1], Kevin M. Douglas[1], John M. C. Plane*[1]

[1] School of Chemistry, University of Leeds.
[+] Now at School of Mechanical Engineering, University of Sheffield.

* corresponding author. Email: j.m.c.plane@leeds.ac.uk

Abstract

Aluminium atoms are injected into planetary upper atmospheres by meteoric ablation. Rapid oxidation by O_2 to AlO is then likely to be followed by reactions with O_3, O_2 and CO_2 to form larger oxides and carbonates, which can also be reduced by atomic O and CO. The reactions listed below were investigated experimentally using both pulsed laser photolysis of an Al precursor in a slow flow reactor, and pulsed laser ablation of an Al target in a fast flow tube, with laser induced fluorescence detection of AlO. The experimental results were interpreted using electronic structure theory calculations and Rice-Ramsperger-Kassel-Markus theory. The low-pressure limiting rate coefficients for the two recombination reactions are: $\log_{10}(k_{rec,0}$ (AlO + O_2 + N_2, 192-812 K)) = -35.137 + 6.1052 $\log_{10}(T)$ - 1.4089 $(\log_{10}(T))^2$; and $\log_{10}(k_{rec,0}$(AlO + CO_2 + N_2, 193-813 K)) = -38.736 + 8.7342$\log_{10}(T)$ - 2.0202 $(\log_{10}(T))^2$ cm^6 $molecule^{-2}$ s^{-1}, with a ±20% uncertainty over the experimental temperature range. The following bimolecular reactions were also studied at 295 K: k(AlO + O_3 → OAlO + O_2) = (1.25 ± 0.19) × 10^{-10}; k(AlO + CO → Al + CO_2) = (1.95 ± 0.35) × 10^{-12}; k(OAlO + CO → AlO + CO_2) = (2.6 ± 0.7) × 10^{-11} and k(OAlO + O → AlO + O_2) = (1.9 ± 0.8) × 10^{-10} cm^3 $molecule^{-1}$ s^{-1}. In the terrestrial atmosphere between 65 and 110 km, AlO is mostly removed by recombination with O_2 below 85 km, and reaction with O_3 above 90 km. On Mars recombination with CO_2 is much more important than with O_2, although reduction of AlO by CO should maintain a significant density of Al atoms. Here we show that in both atmospheres, AlOH is likely to be an important reservoir.

Keywords: Gas-phase Kinetics, Metal Oxides, Aluminum, Aluminum Oxide, Earth upper atmosphere, Mars Upper Atmosphere, Meteoric Ablation.

1. Introduction

Metal atom layers in the mesosphere-lower thermosphere (MLT) altitude region (70 – 110 km) are produced by ablation of the 28 ± 16 tonnes of cosmic dust that enters the terrestrial atmosphere every day.[1] Aluminium (Al) is present in cosmic dust with a relative mass abundance of 9.2×10^{-3}, and an Al:Fe ratio of 0.096.[1] A recent study[1] of cosmic dust sources in the solar system estimates that 14% of the Al in this dust ablates as Al atoms (compared with 36% of Fe). Because Al is mainly present in cosmic dust as a highly refractory oxide, 94% of the ablated Al comes from fast-moving Halley-Type Comets which undergo heating to relatively high temperatures (>2300 K) during atmospheric entry.[1]

Figure 1 shows a partial reaction scheme involving neutral Al species in the MLT (we have investigated the ion-molecule chemistry of Al^+ elsewhere[2]). Ablated Al atoms will be very short-lived in the MLT, because of the rapid reaction with O_2:

$$Al + O_2 \rightarrow AlO + O \qquad \Delta H°(0\ K) = -14 \pm 9\ kJ\ mol^{-1} \qquad (R1)$$

which has a rate coefficient of $k_1(298\ K) = (1.68 \pm 0.24) \times 10^{-10}\ cm^3\ molecule^{-1}\ s^{-1}$.[3] AlO can then go on to react with O_2, CO_2 and O_3 in the MLT:

$$AlO + O_2\ (+ M) \rightarrow OAlO_2 \qquad \Delta H°(0\ K) = -218\ kJ\ mol^{-1} \qquad (R2)$$

$$AlO + CO_2\ (+ M) \rightarrow AlCO_3 \qquad \Delta H°(0\ K) = -157\ kJ\ mol^{-1} \qquad (R3)$$

$$AlO + O_3 \rightarrow OAlO + O_2 \qquad \Delta H°(0\ K) = -291\ kJ\ mol^{-1} \qquad (R4)$$

where M is the bath gas. AlO can also be reduced back to Al by CO (potentially important in a CO_2-rich atmosphere such as Mars and Venus), and OAlO can be reduced back to AlO by either O or CO:

$$AlO + CO \rightarrow Al + CO_2 \qquad \Delta H°(0\ K) = -34\ kJ\ mol^{-1} \qquad (R5)$$

$$OAlO + CO \rightarrow AlO + CO_2 \qquad \Delta H°(0\ K) = -141\ kJ\ mol^{-1} \qquad (R6)$$

$$OAlO + O \rightarrow AlO + O_2 \qquad \Delta H°(0\ K) = -107\ kJ\ mol^{-1} \qquad (R7)$$

The enthalpy changes (at 0 K) in these reactions are calculated at the CBS-QB3 level of theory[4] (see Section 4). Reactions R4 - R7 do not appear to have been studied previously. The rate coefficient for R2 ($AlO + O_2$) has been measured by Belyung and Fontijn,[5] although Ar bath gas was used and the study focused on high temperatures (305 -1690 K). Above 1000 K, the reaction became second-order and this was postulated to be due to a bimolecular channel opening up to form OAlO + O. R3 ($AlO + CO_2$) was studied by Parnis *et al.*,[6] though in a relatively high pressure regime (200 - 700 Torr) with N_2O as the bath gas. In the same study, a slow third-order reaction between AlO and CO was reported.

In the present study we report kinetic measurements of R2 – R7 (depicted in red in Figure 1). Electronic structure calculations are then be used to elucidate the reaction pathways and extrapolate to the low temperatures (120 - 240 K) and pressures (< 5 Pa) in the MLT. In the final part of the paper, the relative rates of the reactions involving AlO are examined as a function of altitude in the atmospheres of Earth and Mars.

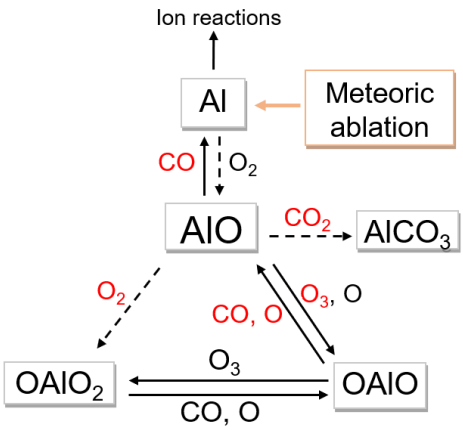

Figure 1. Partial reaction scheme for the neutral chemistry of Al in the MLT. Meteoric ablation provides the initial source of Al. Previously measured reactions are shown by dashed lines, with red species indicating reactions measured in the present study.

2. Experimental

Reactions R2−R4 were studied using the pulsed laser photolysis−laser-induced fluorescence (PLP-LIF) technique within a temperature-controlled reactor. This reactor has been used previously[7] to study the kinetics of a range of mesospheric metals (e.g. Si, Mg, Ca, Fe). For a recent schematic diagram of the experimental layout, see Figure 2 of Mangan *et al.*[8] The stainless steel reactor comprises a central chamber with five side arms and a temperature range of 192 - 1100 K. AlO molecules were produced in the reactor by multiphoton dissociation of aluminium acetylacetonate ($Al(C_5H_7O_2)_3$, also known as $Al(acac)_3$) vapor by a loosely focused KrF excimer laser (Physik COMPEX 102) at 248 nm, with a typical pulse energy of 40 mJ at 10 Hz (< 5 mJ in the reactor). Solid $Al(acac)_3$ powder was inserted into one of the chamber arms in a steel boat attached to the end of a thermocouple (K-type) and heated to ~340 K using heating tape around the reactor arm, in order to achieve a sufficient $Al(acac)_3$ vapour pressure, estimated to be 4.6×10^{-4} Torr.[9] A flow of N_2 over the steel boat entrained and transported the $Al(acac)_3$ vapour into the main reactor volume. Experiments were conducted up to a maximum temperature around 810 K; above this temperature the LIF signal degraded, presumably due to decomposition of the $Al(acac)_3$ precursor on the timescale of its residence in the reactor (~1 s).

The transition probed by LIF was the AlO ($B^2\Sigma^+$ - $X^2\Sigma^+(0,0)$) band at 484.23 nm,[10] using a Nd:YAG (Quantel Q smart 850 at 355 nm) pumped dye laser (Sirah Cobra-stretch CBST-G-18) with Coumarin 102 laser dye. The time delay between the counter-propagating dye laser (probe) and excimer laser (photolysis, $t = 0$) beams was varied to produce scans of the relative AlO concentration with time. Typical kinetic traces were produced from 1000 laser shots, with an accumulation time of 100 s. The AlO LIF signal was collected using a photomultiplier tube (Electron Tubes, model 9816QB) positioned orthogonal to the laser beams, through an interference filter (λ_{max} = 480 nm, fwhm = 10 nm).

A total gas flow through the reactor of 180 sccm included the entrained $Al(acac)_3$ vapor in N_2, reactant gas (O_2, CO_2 or O_3 in N_2) and a balancing flow of the N_2 bath gas. These flows were set using calibrated mass controllers, and the pressure in the reactor (5 – 18 Torr) measured with a capacitance manometer. O_3 was generated by flowing O_2 through a commercial ozoniser and the concentration measured downstream of the reactor by optical absorption at 254 nm (for details see Mangan *et al.*[8]).

Reactions R5 - R7 were studied using a stainless steel fast flow tube reactor (for a schematic diagram see Figure 1 in Daly *et al.*[2]). Pulses of Al atoms were generated in the N_2 carrier gas flow by the laser ablation of a rotating Al rod positioned centrally within the upstream section of the tube, using a loosely focused 532 nm Nd:YAG laser (Continuum Minilite, pulse rate = 10 Hz, pulse energy = 8 mJ). At the downstream end of the tube, AlO was probed by LIF using a Nd:YAG (Continuum Surelite SL1-10 at 355 nm) pumped dye laser (Sirah Cobra). The LIF signal was collected using a boxcar integrator (Stanford Research Systems SR200), and the digital signal transferred via a National Instruments CompactRIO interface. Each experimental data point was produced by an average of 600 laser shots.

Experiments were carried out with a total laminar flow of 3 slm, using a throttled roots blower (Edwards EH500A) backed by an Edwards E2M80 rotary pump to maintain a pressure of 1 Torr at 295 K. The distance from the Al rod to LIF detection point was 455 mm. O_2 and O_3 were introduced through a side-arm in the flow tube, 230 mm upstream from the detection point, while CO and O were introduced at the same distance via a sliding injector. The flow velocity in the tube was set to 67 m s^{-1}, giving a flow time from reactant injection to LIF detection of 3.5 ms. A mixing time for the reactants of 1.5 ms was used, estimated as the time taken for O_3 to diffuse 1 cm across the tube in a laminar flow, with $D(O_3\text{-}N_2)$ = 134 cm^2 s^{-1} at 1 Torr.[11] Atomic O was produced by the microwave dissociation of N_2 followed by titration with NO. We have described previously[12] the method used to determine the absolute O atom concentration at the point of injection, and the subsequent rate of loss on the flow tube walls.

Materials. N_2 (99.9999% pure, Air Products), O_2 (99.999%, pure Air Products), CO_2 (99.995% pure, Air Products) and CO (99.5% pure, Argo International) were used without any further purification. NO (99.95%, Air products) was purified via freeze-pump-thaw cycles before dilution in N_2. $Al(acac)_3$ (99% pure, Sigma Aldrich) was warmed gently under vacuum in the reactor prior to experiments. The Al rod (Alfa Aesar) was 99.999% pure.

3. Results

3.1 AlO + O_2 and CO_2

The time-resolved LIF signals of AlO are described by a single exponential form $A\exp(-k't)$, where the pseudo first-order decay coefficient k' (taking R2 as an example, where O_2 is the reactant) is given by:

$$k' = k_{diff} + k_2[O_2][N_2] \qquad \text{(E1)}$$

k_{diff} is the rate of diffusion of AlO molecules out of the photolysis volume observed by the PMT. Figure 2 shows kinetic traces over a range of $[O_2]$ as a natural logarithm of the raw LIF signal against time, confirming the pseudo first-order behaviour after the first ~200 μs. AlO is produced rapidly after photolysis of the precursor, either directly or by R1 (with an e-folding lifetime of < 2μs at the O_2 concentrations employed). The small rise and plateau in LIF signal before 200 μs is most likely caused by quenching of vibrationally excited AlO, as reported by Parnis *et al.*[6] The time-resolved decays of AlO were fitted at reaction times longer than 300 μs, to ensure that quenching did not affect the retrieved value of k_2. Beginning the analysis at even longer times did not change the retrieved first-order rate within erro, but was avoided in order to maximise the number of datapoints with good signal-to-noise in each fit, thereby reducing the error.

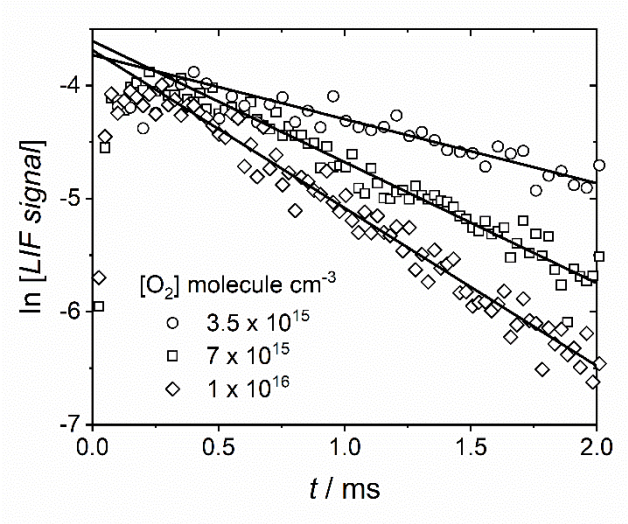

Figure 2. Kinetic decays of AlO reacting with different $[O_2]$ (total pressure = 5.3 Torr). The lines are linear regressions through each decay from ~ 0. 3 ms onwards.

Example plots of k' against $[O_2]$ at temperatures between 300 and 600 K are shown in Figure 3, with the slope providing the second order-rate coefficient at a specific pressure of N_2. The profiles in Figure 3 show non-zero intercepts, with the measured loss rate of AlO in the absence of a reactant typically between 2000 – 5000 s^{-1}. This is several times higher than typical diffusion rates of metal oxides under the experimental conditions of this study and is likely due to removal of AlO by the precursor $Al(acac)_3$, or a precursor fragment produced by thermal decomposition of the precursor.[8] This loss rate was monitored at the start and end of each experimental run, and found to be constant within error.

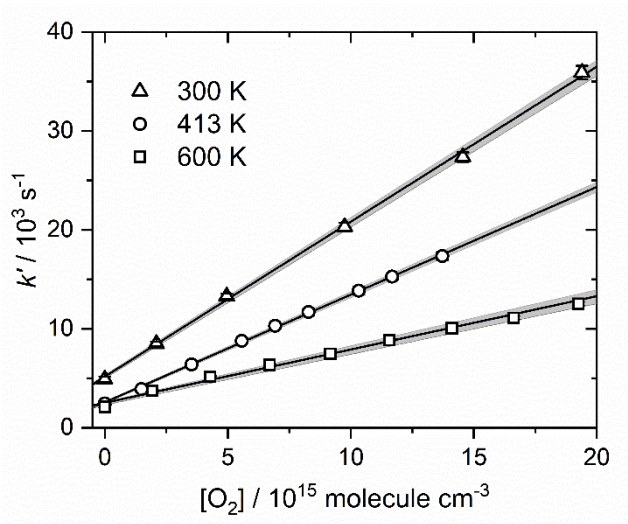

Figure 3. Plots of k' against $[O_2]$ for R2 at 5.3 Torr total pressure for 300 – 600 K. The shaded area indicates the 95% confidence limits for each fit.

Figure 4a shows the pressure dependence of the second-order rate coefficients for R2 and R3 at room temperature. R2 is clearly in the fall-off region over the pressure range studied (5 - 17 Torr) while R3 is linearly pressure-dependent. Figure 4b illustrates the overall negative temperature dependences of R2 and R3. The flattening out of the rate coefficients below 400 K is discussed in Section 4.

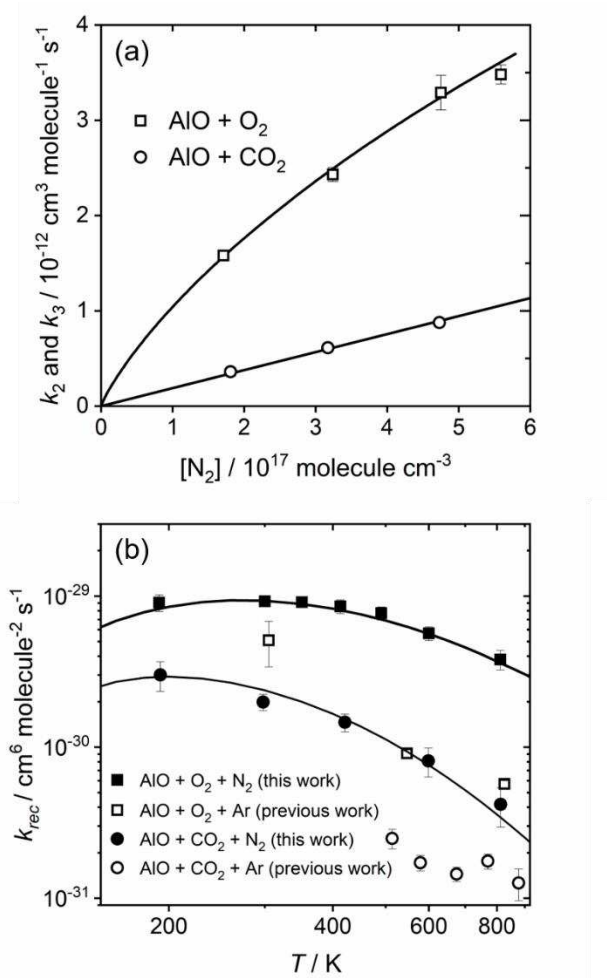

Figure 4. (a) Pressure dependence of k_2 (AlO + O_2) and k_3 (AlO + CO_2) at 300 K in N_2 bath gas. The symbols are experimental values, and the lines are RRKM fits. (b) Third-order rate coefficients for R2 and R3 as a function of temperature. Solid symbols are measurements from the present study at in N_2 pressures of 5.3 and 5.4 torr, respectively. The previous measurements of R2 by Belyung and Fontijn[5] and R3 by Rogowski *et al.*[13] were at Ar pressures between 10 and 20 Torr.

3.2 AlO + O_3

The decay of AlO in the presence of O_3 and O_2 can be described by:

$$k' = k_{diff} + k_4[O_3] + k_2[O_2] \qquad \text{(E2)}$$

A plot of k' as a function of [O_3] is shown in Figure 5. The contribution from R2 (up to 50% at low [O_3]) and the remaining contribution from the non-zero intercept has been subtracted from k' to leave the contribution from R4. The linear dependence of k' with [O_3] indicates the absence of a recycling reaction back to Al, which has been observed for other metal oxides such as NaO and NiO.[7, 8] This is unsurprising, given the very strong bond energy of AlO (503 kJ mol^{-1} [14]). A linear regression fit yields k_4(295 K) = (1.25 ± 0.19) × 10^{-10} cm^3 molecule^{-1} s^{-1}.

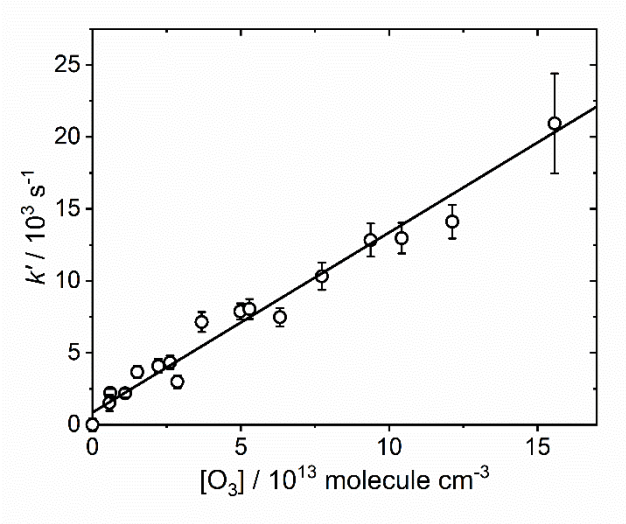

Figure 5. Plot of k' against $[O_3]$ for the reaction of AlO + O_3 (R4) at 295 K. The line is a linear regression through the dataset.

3.3 Flow tube kinetics

R5, R6 and R7 were studied at 295 K and 1 Torr total pressure of N_2, using the flow tube apparatus described in Section 2. AlO was formed from ablated Al atoms via R1 (Al + O_2) in the upstream section of the flow tube where further reagents (e.g. CO, O_3 and O) were also added. Unlike the chemistry in the PLP-LIF system which involved simple pseudo first-order kinetics, the more complex chemistry in the flow tube requires a kinetic model to extract useful kinetic data. For this model a set of coupled ordinary differential equations describing the time-dependent behaviour of the Al species (Al, AlO, OAlO etc.) in the flow tube were solved in order to fit to the experimental data. This flow tube model has been described in detail elsewhere.[15] The rate coefficients for R2 and R4 measured in the present study, and k_1 from our previous study,[3] were used.

Table 1. Parameters and estimated diffusion coefficients for Al species in N_2 at 295 K.

Species	Dipole moment / Debye	Polarizability / 10^{-24} cm^3	Ionization energy / eV	Diffusion coefficient / Torr cm^2 s^{-1}
Al	-	6.8 [a]	5.99 [a]	121
AlO	4.45 [b]	8.6 [c]	9.82 [d]	90.9
OAlO	-	9.0 [c]	9.71 [c]	84.2

[a]Lide *et al.*[16] [b]Bei and Steimle.[17] [c]Calculated at the B3LYP/6-311+g(2d,p) level.[4] [d]Clemmer *et al.*[18]

The diffusional loss rates of Al, AlO and OAlO to the walls of the flow tube were also required, and these were calculated (the diffusion coefficient of AlO could not be measured because of the need for O_2 to be present in the flow tube to produce AlO from ablated Al, so that removal of AlO via R2 was unavoidable). The diffusion coefficients in N_2 and hence wall loss rates (assuming an uptake coefficient on the walls close to unity) for Al, AlO and OAlO were estimated from the long-range capture forces between these species and N_2, a method we have

described elsewhere.[12] The relevant parameters and resulting diffusion coefficients are listed in Table 1.

Time zero in the model is the point where the reactants are mixed into the flow tube, and the model end point is the time when the metal pulse reaches the LIF detection point (~2 ms). The model is initialised by fitting [AlO] to the experimental AlO LIF signal in the absence of the reactant being studied (CO or O) by constraining the initial model [Al]. This is done using the independently measured rate coefficients, reactant concentrations and the calculated diffusion rates at 1 Torr. Due to the fast Al + O_2 reaction, Al is essentially completely converted to AlO within 0.5 ms of O_2 addition. [AlO] reaches a peak at this point in the flow tube and then decreases due to diffusion to the flow tube walls and chemical loss. After initializing the model, the model is run to simulate the conditions of each experimental data point by turning on the CO or O and optimizing the appropriate rate coefficient (k_5, k_6 or k_7) to best fit the AlO LIF signal of that data point. The mean of these optimized fits gives the overall value and standard error of the rate coefficient.

The sensitivity of the model-fitted rate coefficients to realistic uncertainties in the diffusion rates of the Al species, and the uncertainties of previously measured reaction rate coefficients, is not significant. Varying k_1 and k_2 in the case of fitting k_5, and also k_4 for fitting k_6 and k_7, within their respective error limits still produces model simulations that lie well within the scatter of the experimental data. Concerning diffusion, changing the diffusion coefficients for the Al species by an unrealistically large factor of 2 from their calculated values primarily causes a change in the [Al] required to initialize the model, but the model fits remain within the scatter of the experimental data over the range of reactant concentrations. Since the fitting procedure is primarily sensitive to the scatter in the experimental data, the uncertainty in each determined rate coefficient is given by the standard deviation (± 1σ) of the mean of the fitted values to each of the datapoints.

3.4 AlO + CO

This reaction was studied first as k_5 needed to be added to the kinetic model for the subsequent fitting of R6 (OAlO + CO). Just sufficient O_2 was added ($[O_2] = 2.4 \times 10^{13}$ molecule cm^{-3}) to maximise the AlO LIF signal at the downstream detection point, but minimise further reaction with O_2 to produce $OAlO_2$ (R2), or overwhelm recycling of AlO back to Al by R5. This procedure also avoids significant recycling from $OAlO_2$ by CO which would then interfere with the observed AlO as a function of CO. The points in Figure 6 shows the measured AlO signal as a function of added CO, normalised against the signal in the absence of [CO] (i.e., the ratio $[AlO]/[AlO]_0$). The addition of sufficient CO (2.2×10^{14} molecule cm^{-3}) causes an 8.6% reduction in AlO via recycling to Al by R4, which is partially offset by re-oxidation of Al to AlO by R1. The model fit to the dataset (solid line in Figure 6) yields k_5(295 K) = (1.95 ± 0.35) $\times 10^{-12}$ cm^3 molecule^{-1} s^{-1}.

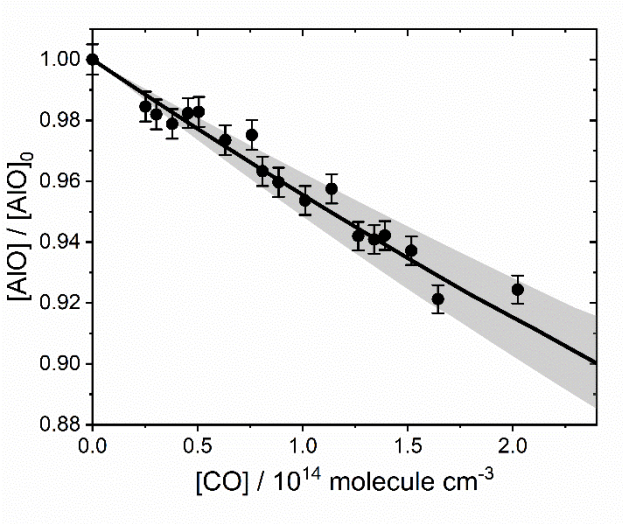

Figure 6. Plot of $[AlO]/[AlO]_0$ against [CO] for the reaction of AlO + CO ($[O_2] = 2.44 \times 10^{13}$ molecule cm^{-3}, 295 K and 1 Torr). The line is the kinetic model fit to the dataset, with the shaded area showing the associated error in the fit (± 1σ).

3.5 OAlO + CO

Once k_5 had been measured, R6 (OAlO + CO) could be investigated. This required the addition of a fixed $[O_3]$ to produce OAlO via R4, while [CO] was varied. The corona discharge converted 1.5% of O_2 into O_3, so that $[O_2]$ (1.01×10^{14} molecule cm^{-3}) was ~33 times larger than the $[O_3]$ (3.28×10^{12} molecule cm^{-3}). Figure 7 shows the observed [AlO] as a function of CO, normalized by $[AlO]_0$, the signal when [CO] = 0. There is a marked increase in the $[AlO]/[AlO]_0$ ratio as [CO] is increased, clear evidence for reduction of OAlO by CO.

However, based on our experience with other metal dioxides,[12] O_3 should in turn oxidize OAlO:

$$OAlO + O_3 \rightarrow OAlO_2 + O_2 \qquad \Delta H°(0\ K) = -226\ kJ\ mol^{-1} \qquad (R8)$$

R8, as well as affecting the concentration of OAlO if the rate were sufficiently fast, would also contribute a kinetically relevant concentration of $OAlO_2$, particularly in combination with direct formation of $OAlO_2$ via R2 ($AlO + O_2$). This makes the flow tube kinetics sensitive to another potential reaction between $OAlO_2$ and CO:

$$OAlO_2 + CO \rightarrow OAlO + CO_2 \qquad \Delta H°(0\ K) = -207\ kJ\ mol^{-1} \qquad (R9)$$

The sensitivity of the value of k_6 retrieved from the model fit to the experimental data was therefore tested with respect to k_8 and k_9. The overall shape of the modelled variation of $[AlO]/[AlO]_0$ with [CO] was not influenced by varying k_8, but an increase in k_8 caused an increase in the fitted value of k_6. As an upper limit to k_8 could therefore not be constrained experimentally, it was set to the measured value for $AlO + O_3$ (i.e. $k_8 \leq 1.25 \times 10^{-10}$ cm^3 $molecule^{-1}$ s^{-1}). This is based on our previous work on Fe oxides which showed a monotonic decrease in the rate coefficients for Fe, FeO and $OFeO + O_3$,[12] and the fact that in this case OAlO is a linear molecule[19] with no dipole moment and hence will have weaker long-range interactions with O_3 compared to AlO.

In contrast, the shape of the modelled variation of $[AlO]/[AlO]_0$ with [CO] is sensitive to k_9: if too large, the model underestimated the AlO signal recovery at low [CO] and overestimated the recovery at high [CO]. This enabled an upper limit of k_9 (295K) $\leq 5 \times 10^{-12}$ cm^3 $molecule^{-1}$

s^{-1} to be obtained. The final fit to k_6 (solid line in Figure 7) was achieved by varying k_8 and k_9 from 0 to their respective upper limits. This produced a 28% uncertainty in the fit to k_6, so that k_6(295 K) = (2.6 ± 0.7) × 10^{-11} cm^3 $molecule^{-1}$ s^{-1}.

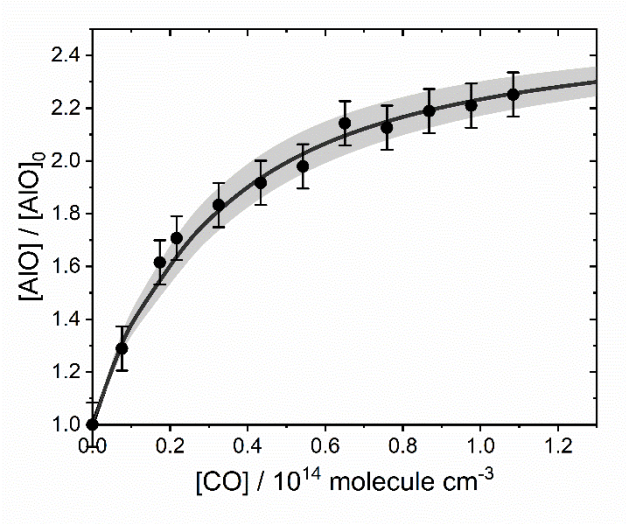

Figure 7. Plot of [AlO]/[AlO]$_0$ against [CO] for the reaction of AlO_2 + CO ([O_2] = 1.08 × 10^{14} molecule cm^{-3}, [O_3] = 3.28 × 10^{12} molecule cm^{-3}, 295 K and 1 Torr). The line is the kinetic model fit to the dataset, with the shaded area showing the associated error in the fit (± 1σ), caused by the variability in R7 and R8 (see text).

3.6 OAlO + O

OAlO was produced in the same way as for studying R6, and the same upper limit for k_8 was used in the kinetic model. However, instead of varying the reactant of interest (in this case O), [O_3] was varied while [O] was fixed to 7.02 × 10^{12} molecule cm^{-3} at the point of injection. This procedure was adopted because it is considerably easier to vary [O_3], which was continuously monitored by optical absorption, than to vary [O] and carry out a new titration with NO_2 at each point. This would require turning off the ozoniser and the Al ablation laser, making the [O] measurement, restarting ablation and O_3 production, and waiting for the signals to stabilize, a process which would take in excess of 30 min and lead to significant signal drift. Figure 8 shows the AlO signal as a function of [O_3] (0.2 – 3.7 × 10^{12} molecule cm^{-3}), in the absence of [O] (open circles) or at fixed [O] (black circles). The measured wall loss of O was 150 ± 22 s^{-1}. O was added from the sliding injector close to the centre of the flow, while the O_3 was added through a side port of the flow tube. As well as the reaction of interest (R7) there are two other possible reactions involving O that could occur in the flow tube:

$$AlO + O\ (+ N_2) \rightarrow OAlO \qquad \Delta H°(0\ K) = -390\ kJ\ mol^{-1} \qquad (R10a)$$

$$\rightarrow OAlO + h\nu \qquad (R10b)$$

$$OAlO_2 + O \rightarrow OAlO + O_2 \qquad \Delta H°(0\ K) = -172\ kJ\ mol^{-1} \qquad (R11)$$

R10a is a termolecular reaction and its rate coefficient is estimated to be k_{10}(295 K) = 7.2 × 10^{-30} cm^6 $molecule^{-2}$ s^{-1}, using the RRKM Master Equation method described in Section 4; hence, this channel is relatively slow at the 1 Torr pressure in the flow tube. The radiative recombination channel R10b, discussed below, also appears to be minor: when O was added to a flow of AlO (and O_2), no change in the AlO LIF signal was observed, suggesting that R10

is too slow to compete with rapid recycling by the bimolecular reaction R7 back to AlO and so was not included in the kinetic model. This cycling between R7 and R10 also makes an independent measurement of R10 difficult in this experimental system. The effect of R11 in the model was well within the scatter of the experimental data points when k_{11} was set to an upper limit $\leq 1 \times 10^{-10}$ cm^3 molecule^{-1} s^{-1}. If a higher value for k_{11} was used, the model failed to reproduce the slope of the experimental data in Figure 8. Indeed, the closest comparable reaction previously studied, $OFeO_2$ + O, was too slow to measure ($< 2.1 \times 10^{-12}$ cm^{-3} molecule s^{-1}) below 466 K.[12] The sensitivity to the O diffusion rate was also investigated, with a doubling of the rate to 300 s^{-1} causing only a 20% increase in the fitted value of k_7. The final model fit through the experimental points, shown by the solid lines in Figure 8, yields k_7(294 K) = (1.9 ± 0.8) × 10^{-10} cm^3 molecule^{-1} s^{-1}.

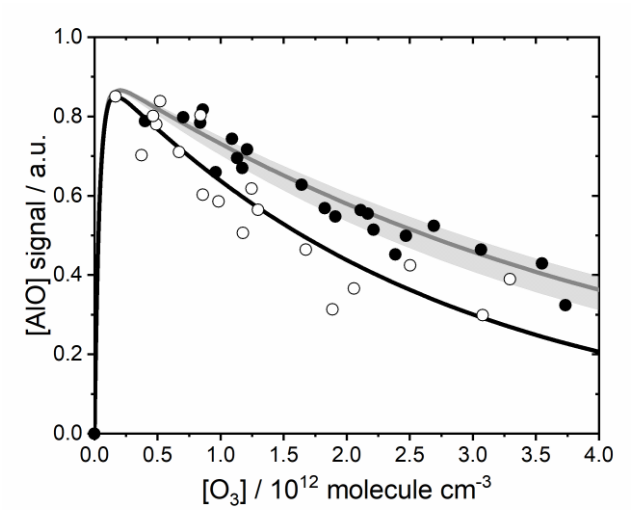

Figure 8. Plots of [AlO] as a function of [O_3] at 1 Torr and 294 K. Solid black circles are experimental data with a fixed addition of O ([O] =7.02 × 10^{12} molecule cm^{-3} at the injection point) and open circles are in the absence of [O]. The solid grey and black lines are the model fits with and without [O], respectively, with the shaded grey area of the model fit representing ± 1σ uncertainty in k_7.

3.6.1 Chemiluminescence from AlO + O

Chemiluminescence produced by R10b was also investigated. This reaction, followed by recycling of OAlO back to AlO (R7) has been hypothesised to explain observations of broad visible emission when Tri-Methyl Aluminium (TMA) grenades are released in the upper atmosphere above 90 km.[20, 21] The LIF detection system was modified by replacing the 480 nm band pass filter with a monochromator, and the PMT used in the photon-counting mode with a multichannel scaler. In order to observe sufficient signal, the slit width of the monochromator had to be set to a width giving a wavelength accuracy of only ± 30 nm, calibrated at 532 nm using a laser diode (Thorlabs CPS532).

The experimental conditions were the same as those used to study the kinetics of R7, but without the addition of O_3 to the flow. A broad emission was seen across the detectable wavelength range (300 – 800 nm) reducing to almost zero at 300 nm, still present at 800 nm, and peaking between 500 - 600 nm. The same profile was observed with just Al and O_2 in the

system, but the raw signal was an order of magnitude higher when [O] was also present and scaled linearly with increasing [O]. A peak observed on top of the broad emission at approximately 400 nm (still present with only Al + N_2 in the flow tube) was attributed to emission from the long lived Al(^{2}S) state, produced by laser ablation of the Al rod, relaxing to the ground state Al(^{2}P).

4 Discussion

The measured second-order rate coefficients as a function of temperature and pressure for R2 – R7 are listed in Table S1 (in the Supporting Information). To understand the unusual behaviour of some of the measured reactions, and to extrapolate the recombination reactions to MLT pressures and temperatures, electronic structure calculations were combined where appropriate with Rice-Ramsperger-Kassel-Markus (RRKM) theory. The geometries of the Al-containing molecules were first optimized at the B3LYP/6-311+g(2d,p) level of theory within the Gaussian 16 suite of programs.[4] More accurate energies were then determined using the Complete Basis Set (CBS-QB3) method.[22] The Cartesian coordinates, rotational constants, vibrational frequencies and heats of formation of the relevant molecules are listed in Table S2. Most of the geometries are illustrated in Figure 9, which shows the potential energy surfaces for R2 (AlO + O_2) and R3 (AlO + CO_2).

The results obtained here are generally in good agreement with previous theoretical work.[23-27] In particular, the most stable isomer of AlO_2 is linear OAlO($^2\Pi_g$), as demonstrated in a photoelectron spectroscopy experiment by Desai *et al.*[19] This study measured the symmetric vibrational frequency to be 810 cm^{-1}, in excellent agreement with our calculated value of 830 cm^{-1} (Table S2). A matrix isolation study by Andrews *et al.*[28] attributed a vibrational frequency at 1129 cm^{-1} to OAlO, but this assignment does not seem to be correct. In contrast, their frequency at 496 cm^{-1} attributed to cyclic AlO_2 agrees well with our calculated value of 504 cm^{-1}. In the case of AlO_3, four absorptions at 838, 850, 853 and 861 cm^{-1} attributed to this isomer are consistent with our calculated values of 859 and 868 cm^{-1}. The matrix study[28] reported an absorption at 964 cm^{-1} for the C_{2v} $OAlO_2$ isomer, which seems quite low compared with our closest vibrational mode at 1109 cm^{-1}.

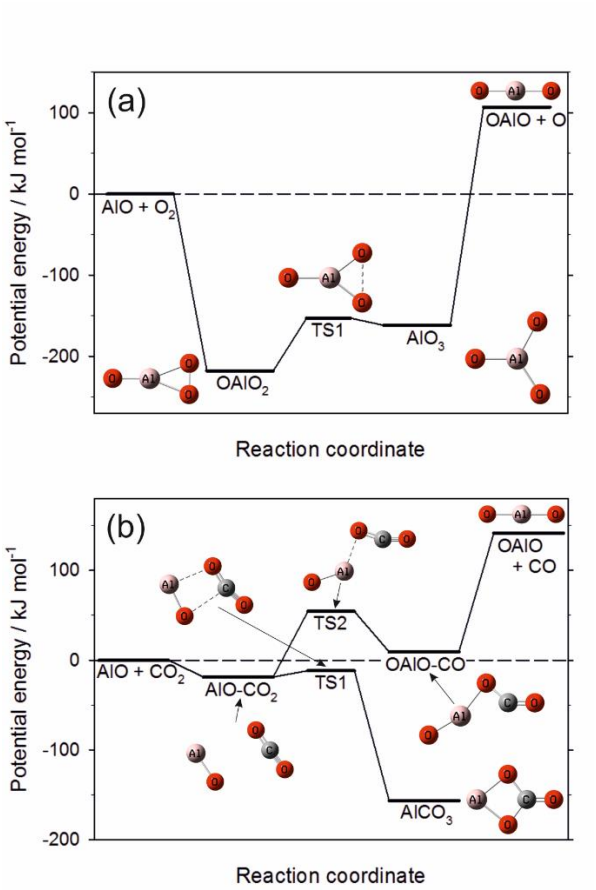

Figure 9. Potential energy surfaces calculated at the CBS-QB3 level of theory: (a) AlO + O_2; (b) AlO + CO_2, where the barrier height of TS1 has been increased by 13 kJ mol^{-1} to optimise the RRKM fit.

4.1 AlO + O_2 and AlO + CO_2

The reaction between AlO and O_2 has been studied previously by Belyung and Fontijn[5] over a wide range of temperature (305 – 1689 K) and pressure (5 – 75 Torr). They found that the reaction was pressure-dependent below 1010 K and, as in the present study, observed clear fall-off behaviour at 305 K. As shown in Figure 4(b), their reported third-order rate coefficients are somewhat slower (e.g. 44% slower around 300 K) than in the present study, which is probably explained by the use of Ar rather N_2 as the bath gas. Above 1000 K, R2 became pressure independent, which was attributed to the bimolecular reaction dominating the kinetics:

$$\text{AlO} + \text{O}_2 \rightarrow \text{OAlO} + \text{O} \qquad \Delta H^\circ(0\text{ K}) = 107\text{ kJ mol}^{-1} \qquad \text{(R12)}$$

The measured rate coefficient was reported to be $k_{12}(1010 – 1689\text{ K}) = 7.7 \times 10^{-10} \exp(-83.1\text{ kJ mol}^{-1}/RT)$. Inspection of the Arrhenius plot (Figure 6 in Belyung and Fontijn[5]) shows that the uncertainty in the activation energy is around 23 kJ mol^{-1}, so that the activation energy is consistent with the reaction endothermicity of 107 kJ mol^{-1} at the CBS-QB3 level (Figure 9), where the uncertainty in the theoretical estimate is probably 15 kJ mol^{-1}.[29] It should be noted that OAlO has a well-known problem with symmetry breaking in its wavefunction, and a high-level theoretical study (at the partially spin-restricted RCCSD(T)/aug-cc-pvqz level of theory) indicates that the linear OAlO ($^2\Pi$) state is around 121 kJ mol^{-1} lower than the lowest

state of cyclic AlO_2 ($^2A_2$).[25] This would decrease the endothermicity of R12 to 87 kJ mol^{-1}, in even better agreement with the experimental activation energy.

The reaction between AlO and CO_2 has been studied previously in Ar bath gas by Rogowski *et al.*[13] between 500 and 1300 K. Those authors assumed that the reaction was bimolecular:

$$AlO + CO_2 \rightarrow OAlO + CO \qquad \Delta H°(0\ K) = 141\ kJ\ mol^{-1} \qquad (R13)$$

and did not consider the possible recombination reaction leading to $AlCO_3$, despite obtaining a small negative temperature dependence for the second-order rate coefficient. Dividing their second-order rate coefficients by their respective Ar concentrations yields the points plotted in Figure 4(b), which are in sensible accord with the present study considering the different bath gas. More recently, Parnis *et al.*[6] studied the AlO + CO_2 reaction at high pressures (200 - 700 Torr) of N_2O. They reported rate coefficients between (1.1 - 1.7) × 10^{-11} cm^3 molecule^{-1} s^{-1} at 296 K, and a slight pressure dependence indicating the reaction was well into the fall-off region.

We now describe using RRKM theory to fit the experimental rate coefficients for reactions R2 – R3. The Master Equation Solver for Multi-Energy well Reactions (MESMER) program[30] was used. Each reaction is assumed to proceed via the formation of an excited adduct, which can either dissociate or be stabilized by collision with the N_2 third body. The internal energy of this adduct was divided into a contiguous set of grains (typical width = 110 cm^{-1}) containing a bundle of rovibrational states. Each grain was then assigned a set of microcanonical rate coefficients for dissociation, which were determined using inverse Laplace transformation to link them directly to $k_{rec,\infty}$, the high pressure limiting recombination coefficient. The density of states of each adduct was calculated with the vibrational frequencies and rotational constants listed in Table S2, without making a correction for anharmonicity, and a classical densities of states treatment for the rotational modes. The probability of collisional transfer between grains was estimated using the exponential down model, where the average energy for downward transitions is designated $\langle\Delta E\rangle_{down}$, and the probabilities for upward transitions are determined by detailed balance.[31] $\langle\Delta E\rangle_{down}$ was assigned a small temperature dependence of the form T^{β}. The collision rate of N_2 with the adduct as a function of temperature, $Z(T)$, was calculated using Lennard-Jones parameters (σ and ε) to characterise the intermolecular potential. The ME, which describes the evolution with time of the adduct grain populations, was then expressed in matrix form and solved to yield the recombination rate constant at a specified pressure and temperature.

The adjustable parameters used to perform a global fit to all the experimental data points for each reaction (Table S1) were $k_{rec,\infty}$, σ, $\langle\Delta E\rangle_{down}$ and β. Table 3 summarises the results. The fitted values of $\langle\Delta E\rangle_{down}$ lie between 310 and 330 cm^{-1} i.e. within the expected range for N_2.[31] Although the value of β is usually between -0.5 and 0.5,[31] the somewhat larger values here are needed to capture the decrease in k_2 and k_3 at temperatures above 450 K. $k_{rec,\infty}$ for reaction R3 is essentially the capture rate between AlO and CO_2, with a small positive temperature. In contrast, $k_{rec,\infty}$ for R2 is a factor of 6 smaller than the capture rate, with the slightly higher temperature dependence. This is explained in Figure 9(a), which shows the potential energy surface for R2 as the AlO approaches the O_2 at different angles of attack. Near-orthogonal reactions, where the angle α (defined in the figure legend) is between 90 and 118°, and near-end-on reactions where α is between 145 and 180°, involve significant barriers. Successful collisions are thus quite sterically constrained. This also justifies the small activation energy (2.3 kJ mol^{-1}) for $k_{rec,\infty}$. For both reactions, the expressions for $Z(T)$ (the values for σ and ε are given in the footnotes to Table 3) are essentially at their collision frequencies.

Table 2. Parameters used in RRKM fits to the kinetics of reactions R2 and R3.

Reaction	$\langle\Delta E\rangle_{down}$ cm^{-1} at 298 K	β [a]	$k_{rec,\infty}$ cm^3 molecule^{-1} s^{-1}	$Z(T)$ [b] cm^3 molecule^{-1} s^{-1}
AlO + O_2	330	1.8	8.5×10^{-11} exp(-277 / T)	3.4×10^{-10} $(T/300)^{0.5}$
AlO + CO_2	310	1.9	5.0×10^{-10} exp(-230 / T)	2.4×10^{-10} $(T/300)^{0.5}$

[a] $\langle\Delta E\rangle_{down}(T) = \langle\Delta E\rangle_{down}(T / 298)^{\beta}$

[b] Collision frequency between the adduct and N_2. For AlO-O_2, σ = 3.6 Å and ε/k_B = 250 K. For AlO-CO_2, σ = 3.0 Å and ε/k_B = 250 K.

Satisfactory fits of the bimolecular rate coefficients for R2 and R3 at 296 K are shown in Figure 4a, and the termolecular rate coefficients $k_{2,rec}$ and $k_{3,rec}$ (at the experimental pressure) are compared in Figure 4b. Figure 9a shows that both $OAlO_2$ and AlO_3 are stable with respect to AlO + O_2, and connected by a transition state 153 kJ mol^{-1} below the reactant entrance channel. Since $OAlO_2$ is 56 kJ mol^{-1} lower in energy than AlO_3, this is the major product below 1000 K. Above 1000 K, the formation of OAlO dominates over recombination even at a pressure of 10 Torr, in accord with the experiments of Belyung and Fontijn.[5]

In the case of R3 (AlO + CO_2), Figure 9b shows that a very weakly bound AlO-CO_2 cluster rearranges over a small barrier to form $AlCO_3$. The height of this barrier needed to be increased by 13 kJ mol^{-1} above the CBS-QB3 value to optimise the RRKM fit at temperatures below 350 K, where the negative temperature dependence of $k_{3,rec}$ becomes smaller. This change in energy is within the expected uncertainty at this level of theory.[31] The alternative rearrangement to OAlO-CO and then OAlO + CO involves a significant barrier that is 54 kJ mol^{-1} above the reactant entrance channel; hence the carbonate is the only product that should form below 1000 K.

$k_{2,rec}$ and $k_{3,rec}$ can now be extrapolated to the low pressure limiting values appropriate for modelling in planetary upper atmospheres. The temperature-dependent rate coefficients are well-fitted by second-order polynomials (note that the coefficients are given to 5 significant figures to preserve numerical precision, not to imply accuracy):

$$\log_{10}(k_{2,rec0}) = -35.137 + 6.1052 \log_{10}(T) - 1.4089 (\log_{10}(T))^2$$

$$\log_{10}(k_{3,rec0}) = -38.736 + 8.7342\log_{10}(T) - 2.0202 (\log_{10}(T))^2$$

The uncertainty over the experimental temperature range (190 – 812 K) is ±20%, based on the experimental uncertainties at the temperature extremes.

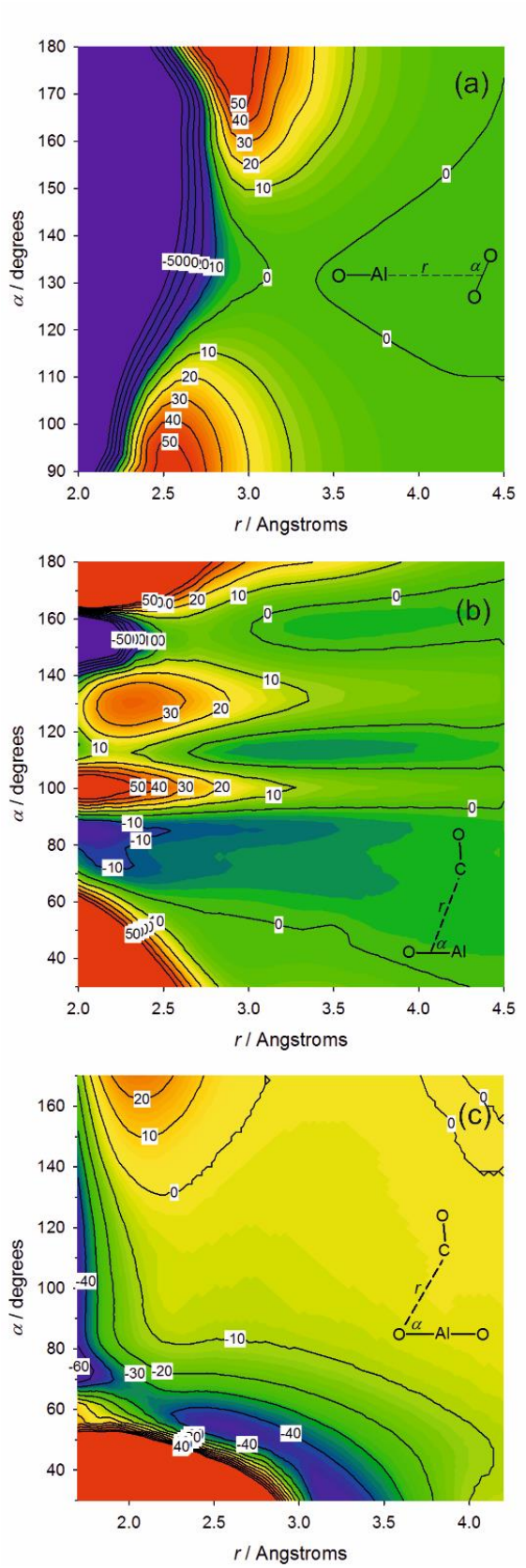

485

486 **Figure 10**. Potential energy surfaces for (a) AlO + O_2, (b) AlO + CO and (c) OAlO + CO,
487 plotted as a function of bond angle α and bond distance r (defined on each figure). Calculations
488 at the B3LYP/6-311+g(2d,p) level of theory. At each (r, α) point on the surface the geometry
489 was optimized with α and r fixed.

4.2 AlO + O_3, CO and O

The reaction between AlO and O_3 is relatively fast: k_4(295 K) = (1.3 ± 0.2) × 10^{-10} cm^3 $molecule^{-1}$ s^{-1} is within a factor of 2 of the rate coefficients for the metal oxides CaO, FeO, KO and NaO which we have studied previously, and 3.7 times faster than MgO + O_3.[7]

The reaction AlO + CO was studied previously by Parnis *et al.*[6] in a high pressure (200 – 700 Torr) of N_2O. They reported a pressure-dependent reaction with a third-order rate coefficient of 4.3 × 10^{-32} cm^6 $molecule^{-2}$ s^{-1}. AlO does indeed form an AlO-CO complex, but this is only bound by 104 kJ mol^{-1} with respect to AlO + CO (at the CBS-QB3 level), and this should then dissociate to Al + CO_2 in a reaction that is overall 34 kJ mol^{-1} exothermic, consistent with our observation of a bimolecular reaction. Insufficient detail is provided in the Parnis *et al*. paper[6] to comment further on this apparent discrepancy. Figure 9b shows the potential energy surface for the approach of AlO to CO. This shows that there are limited angles of attack which allow formation of the AlO-CO complex; this most likely explains why the rate coefficient k_5(295 K) = (1.95 ± 0.35) × 10^{-12} cm^3 $molecule^{-1}$ s^{-1} is significantly slower than the collision frequency.

Garland *et al.*[32] studied the reverse reaction and found that it was bimolecular above 700 K, obtaining k(Al + CO_2 → AlO + CO) = 2.9 × 10^{-10} exp(-(26.8±1.7 kJ mol^{-1}/ RT) cm^3 $molecule^{-1}$ s^{-1}. This activation energy is close to our calculated reaction endothermicity of 34 kJ mol^{-1} at the CBS-QB3 level. This compares well (within the expected uncertainty[29]) with a recent higher level (CCSD(T)/cc-pV(Q+d)) calculation of 21 kJ mol^{-1},[33] and a value of 19 ± 9 kJ mol^{-1} using the currently recommended experimental bond energy (at 0 K) for AlO of 507 ± 9 kJ mol^{-1}.[34] Sun *et al.*[33] showed that there is a submerged barrier on the potential surface connecting AlO with CO, consistent with two crossed molecular beam studies[35, 36] and in disagreement with a previous theoretical study by Sakai[37] who predicted the barrier to lie 79 kJ mol^{-1} above Al + CO_2.

The addition of AlO to O is 390 kJ mol^{-1} exothermic, so that chemiluminescence could potentially be observed down to 306 nm. The broad emission observed in this study is comparable to that seen previously by Golomb and Brown,[38] who added O atoms to a flow of TMA and recorded peak emission at 540 nm. The present study therefore confirms that the emission is produced by reaction 10b.

4.3 OAlO + CO and O

Reaction R6 (OAlO + CO) is relatively fast, about 1 order of magnitude slower than the collision frequency and an order of magnitude faster than R5 (AlO + CO). This is explained by the potential energy surface in Figure 10c, which shows that the reaction is much less sterically constrained compared with R5: attack by CO over a wide range of C-O-Al angles from 60 – 140° should lead to successful reaction.

Reaction R7 (OAlO + O) is close to the collision frequency (k_7 = (1.9 ± 0.8) × 10^{-10} cm^3 $molecule^{-1}$ s^{-1}), and inspection of Figure 9a shows that there are no barriers for this reaction (the reverse of R12). Interestingly, k_7 is a factor 2.3 times faster than the room temperature rate coefficients for the analogous reaction of OMgO, and an order of magnitude faster than the reactions of NaO_2, FeO_2 and CaO_2 with O.[7]

5 Atmospheric Implications for Earth and Mars

The measured rate coefficients for R2 – R5 can now be used to calculate the first-order removal rates of AlO in the atmospheres of Earth and Mars between 65 and 110 km, where Al ablates from cosmic dust particles[1] and has been observed as Al^+ ions on both planets.[2] For Earth, the vertical profiles of T, pressure and the mixing ratios of relevant species (O_3, O_2, CO_2 and CO) were taken from the Whole Atmosphere Community Climate Model (WACCM4),[39] and for Mars from the Mars Climate Database v5.3 ((http://wwwmars.lmd.jussieu.fr/mcd_python/)).[40] For R4 and R5, a $T^{1/6}$ temperature dependence is assumed, typical of a reaction governed by long-range attractive forces. For the recombination reactions in Mars' atmosphere, k_2 and k_3 are multiplied by 2 to account for the increased efficiency of CO_2 compared with N_2.[31]

Figure 11 (top panel) shows that the recombination of AlO with O_2 is the most important loss process below 90 km in the Earth's atmosphere. Above 85 km in the region of the tertiary O_3 maximum,[41] R4 (AlO + O_3) becomes slightly faster as the increasingly low pressure slows down the recombination reaction. Although reduction of AlO back to Al by CO (R5) also becomes competitive above 90 km, the Al product will rapidly be re-oxidized by O_2 (R1), so that this represents a null cycle. The relatively low CO_2 abundance means that R3 (AlO + CO_2) is the slowest of these AlO loss processes between 65 and 110 km.

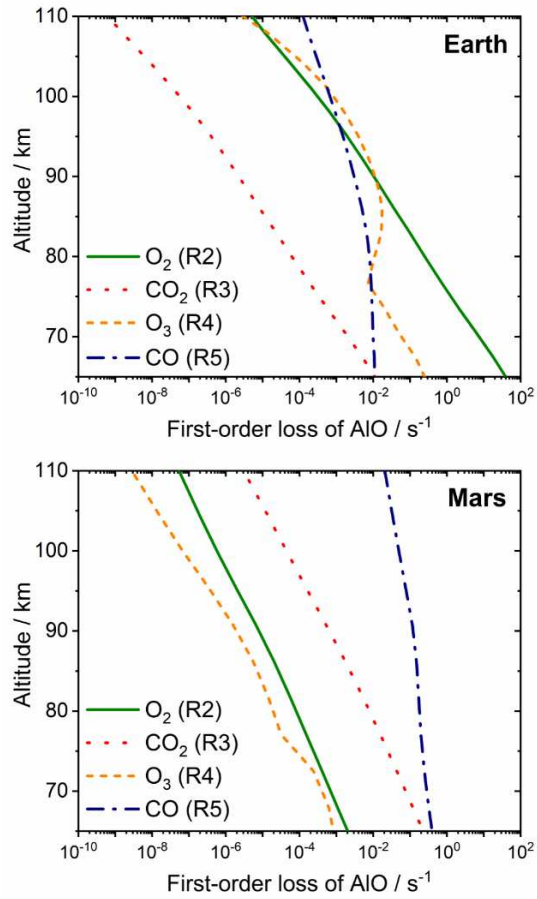

Figure 11. First-order loss rates of AlO by reaction with O_2, O_3, CO_2 and CO (R2 – R5) as a function of altitude in planetary atmospheres: Earth, 40°N, January, local midnight (top panel); Mars, 60°N, solar longitude Ls = 90 (summer solstice), local midnight (bottom panel).

Although this comparison suggests that a primary Al reservoir will be $OAlO_2$, reactions with H_2O and H (which have similar concentrations between 80 and 100 km[7]) will most likely produce AlOH:

$$OAlO_2 + H_2O \rightarrow Al(OH)_2 + O_2 \qquad \Delta H°(0\ K) = -96\ kJ\ mol^{-1} \qquad (R14)$$

$$Al(OH)_2 + H \rightarrow AlOH + H_2O \qquad \Delta H°(0\ K) = -168\ kJ\ mol^{-1} \qquad (R15)$$

$$OAlO_2 + H \rightarrow AlOH + O_2 \qquad \Delta H°(0\ K) = -264\ kJ\ mol^{-1} \qquad (R16)$$

On Mars, the situation is quite different. Figure 11 (bottom panel) shows that recombination of AlO with CO_2 is about 2 orders of magnitude faster than recombination with O_2, and R4 is the slowest reaction because of the relatively low O_3 abundance in Mars' atmosphere. Strikingly, R5 (AlO + CO) dominates AlO removal in the meteor ablation region around 80 km and above. Although the resulting Al atoms will be re-oxidized by O_2, the CO/O_2 ratio is ~3 so that atomic Al should be a significant atmospheric species, with an Al:AlO ratio of ~19. Nevertheless, AlO will still be converted to $AlCO_3$, albeit more slowly because of the recycling between Al and AlO. $AlCO_3$ is then likely to react with O_2, H_2O or H, again producing AlOH:

$$AlCO_3 + O_2 \rightarrow OAlO_2 + CO_2 \qquad \Delta H°(0\ K) = -61\ kJ\ mol^{-1} \qquad (R17)$$

$$AlCO_3 + H_2O \rightarrow Al(OH)_2 + CO_2 \qquad \Delta H°(0\ K) = -158\ kJ\ mol^{-1} \qquad (R18)$$

$$AlCO_3 + H \rightarrow AlOH + CO_2 \qquad \Delta H°(0\ K) = -325\ kJ\ mol^{-1} \qquad (R19)$$

This makes an interesting contrast with the two major metal carbonates, $MgCO_3$ and $FeCO_3$, that should be produced in Mars' atmosphere through meteoric ablation.[1] These carbonates are calculated to have very large dipole moments (11.6 and 9.2 Debye, respectively[42]), so that they bind with up to four CO_2 molecules at the sub-200 K temperatures around 80 km. H_2O then switches with the CO_2 ligands to produce an unreactive hydrated carbonate.[42] The calculated dipole moment of $AlCO_3$ from the present is only 6.5 D; the resulting CO_2 binding energy (32 kJ mol^{-1}) is not strong enough for significant CO_2 cluster formation which would prevent $AlCO_3$ from undergoing reactions R17 – R19.

Finally, unlike other metal hydroxides such as FeOH, NaOH and CaOH,[7, 12, 43] AlOH is stable with respect to reaction with H and O atoms:

$$AlOH + H \rightarrow Al + H_2O \qquad \Delta H°(0\ K) = 60\ kJ\ mol^{-1} \qquad (R20a)$$

$$\rightarrow AlO + H_2 \qquad \Delta H°(0\ K) = 45\ kJ\ mol^{-1} \qquad (R20b)$$

$$AlOH + O \rightarrow AlO + OH \qquad \Delta H°(0\ K) = 56\ kJ\ mol^{-1} \qquad (R20a)$$

and is thus likely to be the major reservoir for ablated Al in both planetary atmospheres.

6. Conclusions

The reactions of AlO with O_2, CO_2 and O_3 were studied using the PLP-LIF technique, and the reactions of AlO with CO, and OAlO with CO and O, using pulsed laser ablation in a fast flow tube. The temperature dependences of the recombination reactions of AlO with O_2 and CO_2 become less negative at temperatures below 350 K, which is explained by small barriers on their potential surfaces. RRKM fits were used to extrapolate the experimental data for these reactions to pressures (< 5 Pa) and temperatures (< 240 K) appropriate for modelling planetary atmospheres. A summary of the measured rate coefficients is provided in Table 3. Chemiluminescence over a broad wavelength range (305 – > 800 nm) was observed from the radiative recombination of AlO with O, presumably by production of electronically excited OAlO. In terms of atmospheric implications, in the Earth's MLT region AlO should be removed most rapidly by O_3 above 85 km and with O_2 below 85 km, with O recycling OAlO to AlO. On Mars, reduction of AlO to Al by CO should maintain a significant Al:AlO ratio. However, in both atmospheres AlOH is predicted to be the major reservoir for meteor-ablated Al.

Table 3. Summary of rate coefficients measured in this study

	Reaction	Rate coefficient[a]
R2	$AlO + O_2$ (+ N_2) → $OAlO_2$	$k_{rec,0} = 10^{-35.137 + 6.1052\log_{10}(T) - 1.4089 (\log_{10}(T))^2}$
R3	$AlO + CO_2$ (+ N_2) → $AlCO_3$	$k_{rec,0} = 10^{-38.736 + 8.7342\log_{10}(T) - 2.0202 (\log_{10}(T))^2}$
R4	$AlO + O_3 \rightarrow OAlO + O_2$	$(1.25 \pm 0.05) \times 10^{-10} (T/295)^{1/6}$
R5	$AlO + CO \rightarrow Al + CO_2$	$(1.95 \pm 0.35) \times 10^{-12} (T/295)^{1/6}$
R6	$OAlO + CO \rightarrow AlO + CO_2$	$(2.55 \pm 0.7) \times 10^{-11} (T/295)^{1/6}$
R7	$OAlO + O \rightarrow AlO + O_2$	$(1.9 \pm 0.8) \times 10^{-10} (T/295)^{1/6}$

[a] Units for termolecular reactions: cm^6 $molecule^{-2}$ s^{-1} (see section 4.1 for uncertainties). Units for bimolecular reactions: cm^3 $molecule^{-1}$ s^{-1}.

Acknowledgements

This work was supported by the UK Natural Environment Research Council (Grant Number NE/P001815/1). The kinetic data and results of theoretical calculations are provided in the Supporting Information.

Supporting Information

Table S1: list of second-order rate coefficients for reactions R2 – R7, as a function of temperature and pressure. Table S2: molecular properties and heats of formation (at 0 K) of AlO, $OAlO_2$, AlO_3, OAlO, and $AlCO_3$, and the stationary points on the AlO + O_2 and AlO + CO_2 potential energy surfaces.

References

1. Carrillo-Sánchez, J. D.; Gómez-Martín, J. C.; Bones, D. L.; Nesvorný, D.; Pokorný, P.; Benna, M.; Flynn, G. J.; Plane, J. M. C. Cosmic dust fluxes in the atmospheres of Earth, Mars, and Venus. *Icarus* **2020,** *335*, art. no.: 113395.

2. Daly, S. M.; Bones, D. L.; Plane, J. M. C. A study of the reactions of Al^+ ions with O_3, N_2, O_2, CO_2 and H_2O: influence on Al^+ chemistry in planetary ionospheres. *Phys. Chem. Chem. Phys.* **2019,** *21*, 14080-14089.

3. Gómez Martín, J. C.; Daly, S. M.; Brooke, J. S. A.; Plane, J. M. C. Absorption cross sections and kinetics of formation of AlO at 298K. *Chem. Phys. Lett.* **2017,** *675*, 56-62.

4. Frisch, M. J.; Trucks, G. W.; Schlegel, H. B.; Scuseria, G. E.; Robb, M. A.; Cheeseman, J. R.; Scalmani, G.; Barone, V.; Petersson, G. A.; Nakatsuji, H., et al. *Gaussian 16, Revision B.01*, Gaussian, Inc.: Wallingford, CT, USA, 2016.

5. Belyung, D. P.; Fontijn, A. The AlO + O_2 Reaction System over a Wide Temperature Range. *J. Phys. Chem.* **1995,** *99*, 12225-12230.

6. Parnis, J. M.; Mitchell, S. A.; Kanigan, T. S.; Hackett, P. A. Gas-phase reactions of aluminum monoxide with small molecules. *J. Phys. Chem.* **1989,** *93*, 8045-8052.

7. Plane, J. M. C.; Feng, W.; Dawkins, E. C. M. The Mesosphere and Metals: Chemistry and Changes. *Chem. Rev.* **2015,** *115*, 4497-4541.

8. Mangan, T. P.; McAdam, N.; Daly, S. M.; Plane, J. M. C. Kinetic Study of Ni and NiO Reactions Pertinent to the Earth's Upper Atmosphere. *J. Phys. Chem. A* **2019,** *123*, 601-610.

9. Frankhauser, W. A. Vapor Pressure Studies on Metal Chelates. Air Force Inst. Tech., Wright-Patterson AFB OH 1965.

10. Saksena, M. D.; Deo, M. N.; Sunanda, K.; Behere, S. H.; Londhe, C. T. Fourier transform spectral study of $B^2\Sigma^+$–$X^2\Sigma^+$ system of AlO. *J. Molec. Spectr.* **2008,** *247*, 47-56.

11. Langenberg, S.; Carstens, T.; Hupperich, D.; Schweighoefer, S.; Schurath, U. Technical note: Determination of binary gas phase diffusion coefficients of unstable and adsorbing atmospheric trace gases at low temperature – Arrested Flow and Twin Tube method. *Atmos. Chem. Phys.* **2020,** *20*, 3669–3682.

12. Self, D. E.; Plane, J. M. C. A kinetic study of the reactions of iron oxides and hydroxides relevant to the chemistry of iron in the upper mesosphere. *Phys. Chem. Chem. Phys.* **2003,** *5*, 1407–1418.

13. Rogowski, D. F.; English, A. J.; Fontijn, A. A high-temperature fast-flow-reactor kinetics study of the reaction AlO + CO_2 → AlO_2 + CO. Thermochemical implications. *J. Phys. Chem.* **1986,** *90*, 1688-1691.

14. Johnson III, R. D. NIST Computational Chemistry Comparison and Benchmark Database *NIST Standard Reference Database* [Online], 2016. http://cccbdb.nist.gov (accessed 1 July 2020).

15. Bones, D. L.; Daly, S. M.; Mangan, T. P.; Plane, J. M. C. A study of the reactions of Ni^+ and NiO^+ ions relevant to planetary upper atmospheres. *Phys. Chem. Chem. Phys.* **2020,** *22*, 8940-8951.

16. Lide, D. R. *Handbook of Physics and Chemistry*. CRC Press: Boca Raton, FL, 2006; Vol. 87th. edn.

17. Bai, X.; Steimle, T. C. The Stark Effect, Zeeman Effect, and Transition Dipole Moments for the $B^2\Sigma^+$–$X^2\Sigma^+$ Band of Aluminum Monoxide, AlO. *Astrophys. J.* **2020,** *889*, art. no.: 147.

18. Clemmer, D. E.; Weber, M. E.; Armentrout, P. B. Reactions of $Al^+(^1S)$ with NO_2, N_2O and CO_2 - thermochemistry of AlO and AlO^+. *J. Phys. Chem.* **1992,** *96*, 10888-10893.

19. Desai, S. R.; Wu, H. B.; Rohlfing, C. M.; Wang, L. S. A study of the structure and bonding of small aluminum oxide clusters by photoelectron spectroscopy: $Al_xO_y^-$ (x=1-2, y=1-5). *J. Chem. Phys.* **1997,** *106*, 1309-1317.

20. Rosenberg, N. W.; Golomb, D.; Allen Jr., E. F. Chemiluminescent techniques for studying nighttime winds in the upper atmosphere. *J. Geophys. Res.* **1963,** *68*, 3328-3330.

21. Rosenberg, N. W.; Golomb, D.; Allen Jr., E. F. Chemiluminescence of trimethyl aluminum released into the upper atmosphere. *J. Geophys. Res.* **1963,** *68*, 5895-5898.

22. Montgomery, J. A.; Frisch, M. J.; Ochterski, J. W.; Petersson, G. A. A complete basis set model chemistry. VII. Use of the minimum population localization method. *J. Chem. Phys.* **2000,** *112*, 6532-6542.

23. Politzer, P.; Lane, P.; Grice, M. E. Energetics of Aluminum Combustion. *J. Phys. Chem. A* **2001,** *105*, 7473-7480.

24. Pak, M. V.; Gordon, M. S. The potential energy surfaces for AlO_2 using multi-reference wave functions. *Chem. Phys. Lett.* **2001,** *344*, 236-240.

25. Pak, M. V.; Gordon, M. S. Potential energy surfaces for the Al + O_2 reaction. *J. Chem. Phys.* **2003,** *118*, 4471-4476.

26. Schnöckel, G. S. a. H. The Molecules AlO_2, $Al(O_2)_2$, and $Al(O_2)_3$: Experimental and Quantum-Chemical Investigations on the Oxidation of Aluminum Atoms. *Angew. Chem. Int. Ed.* **2005,** *44*, 4261-4264.

27. Patzera, A. B. C.; Chang, C.; Sedlmayr, E.; Sülzle, D. A density functional study of small Al_xO_y (x, y = 1−4) clusters and their thermodynamic properties. *Eur. Phys. J. D* **2005,** *32*, 329–337.

28. Andrews, L.; Burkholder, T. R.; Yustein, J. T. Reactions of Pulsed-Laser Evaporated Aluminum Atoms with Oxygen. Infrared Spectra of the Reaction Products in Solid Argon. *J. Phys. Chem.* **1992,** *96*, 10182-10189.

29. Foresman, J. B.; Frisch, Æ. *Exploring Chemistry with Electronic Structure Methods 3rd. ed.* Gaussian, Inc.: Wallingford, CT, 2015.

30. Glowacki, D. R.; Liang, C.-H.; Morley, C.; Pilling, M. J.; Robertson, S. H. MESMER: An Open-Source Master Equation Solver for Multi-Energy Well Reactions. *J. Phys. Chem. A* **2012,** *116*, 9545−9560.

31. Gilbert, R. G.; Smith, S. C. *Theory of Unimolecular and Recombination Reactions*. Blackwell: Oxford, 1990.

32. Garland, N. L.; Douglass, C. H.; Nelson, H. H. Pressure and Temperature Dependence of the Kinetics of the Reaction Al+CO_2. *J. Phys. Chem.* **1992,** *96*, 8390-8394.

33. Sun, Z.; III, K. B. M.; III, H. F. S. The Al + CO_2 →AlO + CO reaction: Experiment vs. theory. *J. Chem. Phys.* **2017,** *147*, art. no.: 171101.

34. Johnson III, R. D., NIST Computational Chemistry Comparison and Benchmark Database, Release 20. In *NIST Standard Reference Database Number 101*, National Institute of Standards and Technology: Gaithersburg, MA, 2019.

35. Costes, M.; Naulin, C.; Dorthe, G.; Vaucamps, C.; Nouchi, G. Dynamics of the reactions of aluminium atoms studied with pulsed crossed supersonic molecular beams. *FaradayDiscuss. Chem. Soc.* **1987,** *84*, 75-86.

36. Honma, K.; Hirata, D. Reaction dynamics of Al + CO_2 → AlO + CO studied by a crossed-beam velocity map imaging technique. *J. Chem. Phys.* **2017,** *147*, art. no.: 013903.

37. Sakai, S. Theoretica Studies on the Chemical Reaction Mechanisms of an Al Atom with the CO_{-2} Molecule. *J. Phys. Chem.* **1992,** *96*, 131-135.

38. Golomb, D.; Brown, J. H. Chemiluminescence of trimethyl aluminum in active oxygen and nitrogen. *Combust. Flame* **1976,** *27*, 383-389.

39. Marsh, D. R.; Mills, M. J.; Kinnison, D. E.; Lamarque, J.-F.; Calvo, N.; Polvani, L. M. Climate Change from 1850 to 2005 Simulated in CESM1(WACCM). *J. Climate* **2013,** *26*, 7372-7391.

40. Forget, F.; Hourdin, F.; Fournier, R.; Hourdin, C.; Talagrand, O.; Collins, M.; Lewis, S. R.; Read, P. L.; Huot, J.-P. Improved general circulation models of the Martian atmosphere from the surface to above 80 km. *J. Geophys. Res.-Planets* **1999,** *104*, 24155-24175.

41. Marsh, D.; Smith, A.; Brasseur, G.; Kaufmann, M.; Grossmann, K. The existence of a tertiary ozone maximum in the high-latitude middle mesosphere. *Geophys. Res. Lett.* **2001,** *28*, 4531-4534.

42. Plane, J. M. C.; Carrillo-Sánchez, J. D.; Mangan, T. P.; Crismani, M. M. J.; Schneider, N. M.; Määttänen, A. Meteoric Metal Chemistry in the Martian Atmosphere. *J. Geophys. Res.-Planets* **2018,** *123*, 695-707.

43. Gómez-Martín, J. C.; Seaton, C.; Miranda, M. P.; Plane, J. M. C. The Reaction between Sodium Hydroxide and Atomic Hydrogen in Atmospheric and Flame Chemistry. *J. Phys. Chem. A* **2017,** *121*, 7667−7674.

Graphical abstract: